Int. J. Solids Structures Vol. 23, No. 7, pp. 947–968, 1987
Printed in Great Britain.

0020-7683/87 $3.00 + .00

ON MODELING OF MECHANICAL PROPERTY CHANGES DURING FLAT ROLLING OF ALUMINUM

PAUL R. DAWSON
Sibley School of Mechanical and Aerospace Engineering, Cornell University, 254 Upson Hall, Ithaca, NY 14853-7501, U.S.A.

(*Received* 17 *April* 1986; *in revised form* 25 *August* 1986)

Abstract—Steady-state rolling of aluminum slabs has been studied with a forming model that assumes rate-dependent plastic flow of the aluminum. Hardening behavior is represented with an internal variable constitutive equation in which parameters are evaluated from independent mechanical property data. Rolling conditions over a broad range of reductions and temperatures were simulated. Computed differences in the resulting property (state) changes and temperature rises are reported. The computed hardness for the lowest temperature simulations are compared to measured yield strengths for rolled aluminum.

NOTATION

a_0	constitutive model parameter
c_0	constitutive model parameter
c_p	specific heat
$\mathbf{d}$	rate of deformation (stretching)
d'_{II}	effective rate of deformation, $(2/3\ \text{Tr}\ (\mathbf{d}\cdot\mathbf{d}))^{1/2}$
$[D]$	matrix of effective viscosities
e	internal energy per unit mass
f_0	constitutive model parameter
$\{F\}$	force matrix
$\mathbf{g}$	gravitational vector
G_e	elastic shear modulus
$[G]$	incompressibility constraint matrix
h	convection coefficient (film coefficient)
$\{h\}$	trace operator
$[H]$	heat transfer coefficient matrix
δJ	virtual rate of work
k	thermal conductivity
$[K]$	shear stiffness matrix
m, m', M	constitutive model parameters
n	constitutive model parameter
$[N], [N_p]$	shape function matrices
$[N'], [N^*]$	shape function spatial gradient matrices
p	Lagrange multiplier (negative of the mean stress)
$\{P\}$	nodal point values of p
$\mathbf{q}$	heat flux
$\bar{q}$	imposed heat flux on S_q
Q_0, Q'_0	thermal activation energies in the constitutive model
$\dot{Q}$	volumetric heat generation rate
$\{Q\}$	thermal source and surface heat flux matrix
S	surface
S_i	portion of the surface having imposed internal variable
S_q	portion of the surface having imposed internal heat flux
S_v	portion of the surface having imposed velocity
S_σ	portion of the surface having imposed traction
S_θ	portion of the surface having imposed temperature
t	time
$\mathbf{T}$	surface tractions
$\bar{\mathbf{T}}$	imposed surface tractions on S_σ
$\mathbf{u}$	velocity
$\bar{\mathbf{u}}$	imposed velocity on S_u
u_{α_t}	tool velocity tangent to the surface
u_s	component of velocity tangent to the streamline
u_t	component of surface velocity tangent to the surface

$\{U\}$	nodal point values of u
V	volume
W	weighted residual for the heat transfer solution
$\mathbf{x}$	spatial coordinates
x_s	coordinate along a streamline.

Greek symbols

β	friction coefficient
η	surface normal
θ	temperature
$\bar{\theta}$	imposed temperature on S_θ
θ_{ref}	reference temperature
θ_m	melt temperature
θ_∞	ambient temperature
θ_0	initial temperature
κ	internal variable
$\bar{\kappa}$	imposed value of κ on S_1
λ	constitutive model parameter
μ_e	effective viscosity
ρ	mass density
$\boldsymbol{\sigma}$	Cauchy stress
σ^*	hardness (internal variable, κ) in Hart's model
σ'_{11}	effective stress, $(3/2\ \mathrm{Tr}\ (\boldsymbol{\sigma}\cdot\boldsymbol{\sigma}))^{1/2}$
τ	yield stress.

Superscripts

$'$	deviatoric quantities
p	plastic elements in Hart's model
v	viscous elements in Hart's model.

Subscript

e	elemental quantities.

1. INTRODUCTION

In the early stages of reducing an aluminum bloom to product forms such as plates, sheets or foil, rolling is performed at elevated temperatures. Elevated temperatures reduce the flow stress necessary to deform the workpiece and increase its ductility, thereby making larger reductions on a given pass possible. At high temperatures the rate dependencies associated with plastic flow are important and thus the material is often modeled as viscoplastic. Further, in the brief time required to compress a slab between the rolls, the flow stress may increase significantly because of strain hardening. In the hot working regime, there is usually sufficient time between passes for recrystallization and recovery processes to reduce the flow stress. The material hardens during each pass and then recovers to a lower flow stress in the time between passes. In the warm working regime, however, the temperatures are usually too low for recovery mechanisms to significantly affect the accumulation of crystal defects that produce higher strength of the workpiece. In either case the workpiece experiences an increase in flow stress during forming as a result of strain hardening. This change in the flow stress is not uniform through the slab since the plastic deformations that produce strain hardening vary through the thickness.

The focus of this paper is the modeling of warm or hot rolling of aluminum with an internal (state) variable constitutive model that assumes isotropic strain hardening. The model parameters have been evaluated from independent laboratory data for aluminum over the regime of temperature, strain, and strain rate that is characteristic of warm and hot rolling. A number of rolling simulations were performed that span a wide range of rolling reductions, temperatures, and frictional conditions. Of particular interest from the results of these simulations are the computed differences in the internal (state) variable of the constitutive model. The state variable represents the material "hardness" and is a measure of the internal dislocation structure of the material. The computed values of the hardness are compared to measured yield strengths of rolled aluminum.

The remaining portion of this section of the paper is devoted to a brief review of related modeling efforts. Subsequent sections review the governing equations, describe the

constitutive model and the evaluation of the parameters needed in the model, summarize the approach taken to solve the equations numerically, and discuss in detail the rolling simulations.

A complete analysis of a solid undergoing large strain deformations during forming processes would necessarily include both elastic and inelastic deformations. Numerical formulations that incorporate elastoplastic material behavior and geometric nonlinearities were first developed in the early 1970s by Hibbit *et al.* (1970) and Needleman (1972) as extensions of existing small strain elastic–plastic formulations. Formulations that have evolved from these early efforts have been used to analyze metal forming processes, including rolling in both two and three dimensions (Kiefer and Hilton, 1985; Kiefer, 1984) in which the plastic deformations may occur both from rate-independent plastic and rate-dependent viscous straining. Other approaches also have been developed such as the formulations based on Lagrangian convected coordinates (Needleman, 1982; Needleman and Tvergaard, 1983; Pierce *et al.*,1983) for both rate-independent and rate-dependent plasticity models and an Eulerian representation in which the reference state is updated with each increment of the deformation so that at the beginning of each increment the current and reference configurations coincide (McMeeking and Rice, 1975). The former approach has been applied to a variety of strain localization problems, as discussed in the cited references. The latter approach has been used by several other investigators to model forming processes, such as extrusion, with rate-independent models (Lee *et al.*, 1977a,b) and rate-dependent models (Chandra and Mukherjee, 1984). Dynamic formulations have also been employed to simulate forming operations with elastoplastic material models, such as the analyses by Key *et al.* (1979) and Flower and Hallquist (1986) on rolling, extrusion and forging processes.

In many forming applications the plastic strains are sufficiently large that it is not necessary to consider the combined elastic and inelastic behavior for analyzing many aspects of the deformation process. Rather, the elastic strains can be neglected and the strains then are taken to be completely inelastic. Kobayashi and co-workers lead this approach, modeling the material as rigid–plastic or rigid–viscoplastic (an extensive summary of these efforts is given by Kobayashi (1985)). Rigid–plastic analyses of rolling have been performed by Li and Kobayashi (1981, 1984), Mori *et al.* (1982), and Estivalet *et al.* (1982). In these analyses, the flow stress increases with the deformation as a function of the accumulated strains. Coupling of the solutions for the flow field and the temperature distribution have been reported by Dawson and Thompson (1977), Zienkiewicz *et al.* (1981), Rebelo and Kobayashi (1980a,b), and Dawson (1980) for extrusion, rolling, forging and welding processes. Argyris *et al.* (1980) have reported on a detailed comparison of the results predicted using elastoplastic and viscoplastic formulations for extrusion and cold-heading processes.

The above-mentioned articles using viscoplastic approximations have assumed either strain hardening behavior for the flow stress at low temperatures or purely viscoplastic behavior at high temperatures. Using a viscoplastic model with a hyperbolic dependence between stress and the rate of deformation, Dawson (1984) showed that in warm and hot rolling processes, the material would be expected to be deformed in a regime of stress and temperature where strain hardening is important, but in which the material would not be well characterized as rate independent. Further, Eggert and Dawson (1986) compared detailed experimental records of the temperature and deformation during upset (solid-state) welding of stainless steel rods to the corresponding histories computed with a purely viscoplastic representation. While the model was reasonably accurate without strain hardening (since the process was compressive and the model was based on peak flow stress data) several features of the comparison suggest that strain hardening plays an important role in the deformation history of the rods. Internal variable plasticity models (as are discussed in more detail later) have been utilized to characterize this more complicated material response by Dewhurst and Dawson (1984) and by Chandra and Mukherjee (1984). This paper provides a detailed examination of the use of an internal variable constitutive model to simulate flat rolling. In addition, it will be shown that this modeling approach can be used to predict the manner in which the material properties, as manifested by the internal variable, change with rolling conditions.

2. EQUATIONS GOVERNING THE FORMING PROCESS

The motion and temperature of the workpiece are governed by balance laws for mass, momentum, and energy. Written in a Eulerian reference frame these relationships are:

conservation of mass
$$\frac{D\rho}{Dt} + \rho \operatorname{div} \mathbf{u} = 0 \tag{1}$$

balance of linear momentum
$$\operatorname{div} \boldsymbol{\sigma} + \rho \mathbf{g} = 0 \tag{2}$$

conservation of energy
$$\rho \frac{De}{Dt} + \operatorname{div} \mathbf{q} - \dot{Q} = 0. \tag{3}$$

A number of assumptions have been made in writing eqns (1)–(3) as they appear above. There is no mass production in eqn (1); inertia has been neglected and there is no momentum production in eqn (2); and in eqn (3) the heat generation includes a contribution from viscous dissipation. The stress $\boldsymbol{\sigma}$ is the Cauchy stress and is symmetric.

Constitutive equations are required to characterize the material behavior mathematically. For the model described herein, the internal energy, heat flux, and stress are written as functions of the rate of deformation, temperature, and state of the material as described by a collection of internal variables:

$$e = e(\mathbf{d}, \theta, \operatorname{grad} \theta, \kappa) \tag{4}$$

$$\mathbf{q} = \mathbf{q}(\mathbf{d}, \theta, \operatorname{grad} \theta, \kappa) \tag{5}$$

$$\boldsymbol{\sigma} = \boldsymbol{\sigma}(\mathbf{d}, \theta, \operatorname{grad} \theta, \kappa). \tag{6}$$

Simple linearized forms of eqns (4) and (5) are assumed to represent the material adequately

$$\frac{D}{Dt}(e) = c_p \frac{D}{Dt}(\theta) \tag{7}$$

and

$$\mathbf{q} = -k \operatorname{grad} \theta. \tag{8}$$

In these forms, the specific heat and conductivity often are specified as functions of temperature, however.

The mechanical behavior is nonlinear and considerably more complex. The constitutive equations for the stress are required to describe the rate-dependent plastic flow of the metal workpiece. Of particular interest is the hardening and recovery behavior exhibited by metals over the regime of stress, strain, and temperature observed in primary forming processes such as rolling. The plastic deformations are assumed to be incompressible, leaving the density constant and reducing the conservation of mass equation to

$$\operatorname{Tr} \mathbf{d} = 0. \tag{9}$$

The constitutive equations for the shear stress behavior accommodate the rate dependency, strain hardening, and temperature sensitivity through a set of equations equivalent to eqn (6) plus any evolution relationships that are necessary. Numerous forms have been published in the literature, as will be mentioned in the following section.

Boundary conditions are necessary to complete the mathematical formulation describing the motion and heating of the workpiece. For the motion, known tractions or velocities are imposed on the surface

$$\boldsymbol{\sigma}\cdot\boldsymbol{\eta} = \bar{\mathbf{T}} \qquad \text{on } S_\sigma \tag{10}$$

and

$$\mathbf{u} = \bar{\mathbf{u}} \qquad \text{on } S_u. \tag{11}$$

In the case of sliding friction over a portion of the boundary, the tangential component of the traction is defined in terms of the relative velocity between the workpiece and the tool

$$\bar{T}_t = \beta(u_\infty - u_t). \tag{12}$$

Boundary conditions for the temperature include known heat fluxes or temperatures on the surface:

$$k \text{ grad } \theta\cdot\boldsymbol{\eta} = \bar{q} \qquad \text{on } S_q \tag{13}$$

and

$$\theta = \bar{\theta} \qquad \text{on } S_\theta. \tag{14}$$

Convective losses on the surface are assumed to be proportional to the difference between the surface temperature and an ambient temperature

$$\bar{q} = h(\theta - \theta_\infty). \tag{15}$$

Finally, boundary conditions must be specified for the internal variables. Everywhere that material enters the Eulerian region known values of the internal variables are imposed

$$\kappa = \bar{\kappa} \qquad \text{on } S_1. \tag{16}$$

(Note that it is mathematically acceptable to impose $\bar{\kappa}$ for a material particle at any point along its streamline through the region. We assume that κ is known as the material enters the region and subsequently evolves with the deformations.)

3. CONSTITUTIVE MODEL FOR PLASTIC DEFORMATIONS OF THE WORKPIECE

The plastic behavior of polycrystalline metals is very complicated. The flow stress depends on the temperature, rate of deformation, and in some way on the past deformations. The change in flow stress that accompanies a change in strain is the difference between the hardening, which results from the accumulation of crystal defects, and softening, which may be a consequence of recrystallization or of rearrangement into stable sub-structures having lower flow stresses (recovery). Hardening essentially occurs concurrently with deformation, while the softening may require much longer times and is strongly dependent on the material's temperature and deformation history. From a modeling viewpoint, it is important to include hardening in the material description because in applications such as rolling the deformations occur in much shorter times than are needed to reduce the flow stress by recrystallization or recovery (Hatch, 1984). Evidence of the increase in flow stress with strain at hot or warm working temperatures is documented in a variety of papers, including data for aluminum (Hockett, 1976; Sheppard and Wright, 1979) and steel (Cook, 1957; McQueen *et al.*, 1975). The data reported by Cook for steel and Hockett for aluminum particularly illustrate such behavior as it relates to hot or warm working. Over the span of temperatures and rates of deformation commonly used in hot working, these materials are observed to strain harden significantly for strains up to approximately 1.0. Although the assumption often is made that the flow stress will saturate at larger strains (and thus strain hardening can be neglected once the material has experienced the first few passes in rolling), Hecker and Stout (1984) reported continued hardening at low temperatures to strains

approaching 7.0, with no apparent trend toward saturation of the flow stress. At high temperatures where recovery or recrystallization is important, the time between passes is sufficient to allow the flow stress to recover a value lower than the saturation stress. In that case each pass begins with a material that exhibits hardening when deformed.

The complexity of the material behavior has important implications for the modeling of bulk forming processes. The assumed constitutive behavior for the plastic flow must be accurate in the regime of temperature, strain rate, and stress that exists in the material as it is processed. In an earlier article (Dawson, 1984), the stress and temperature histories that material particles experience during forming were compared to observed modes of deformation by plotting the stress/temperature trajectories of material particles on a deformation mechanism map. Such maps delineate the dominant modes of deformation as functions of stress and temperature. Although the maps in no way specify the functional forms for the various mechanisms, they do provide an effective means of assessing whether or not a constitutive relationship has been used within the range of conditions that motivated and supported its development. This was done for the case of the slab rolling of an aluminum plate using a viscoplastic model to represent the behavior of the aluminum, as suggested by Sheppard and Wright (1979). The response of the aluminum as it traveled through the process was superimposed on an appropriate deformation mechanism map for several particle paths. While the particles remained well removed from the rate-independent regime (low temperatures and high stresses), it was clear that the conditions were not restricted to such high temperatures that hardening could always be neglected. Thus, constitutive equations that embody hardening, and possibly recovery, are necessary to accurately characterize the material in this and other similar forming processes.

A wide variety of constitutive models has been developed in the past to characterize the plastic flow of polycrystalline metals. This article focuses on plastic behavior that is inherently rate-sensitive since the principal interests are in hot or warm working processes. Simple extension of rate-dependent (viscoplastic) models have been suggested which, for instance, have proposed multiplicative strain and strain-rate functions. Such models are not sufficiently general (because plastic strain is not a true state variable). As alternatives to such models, several internal (state) variable, viscoplastic models have been proposed (see Swearengen *et al.* (1985) for a general review). These models are continuum representations and are phenomenological in their basic foundations. Their structure permits changing load paths, strain rates, and temperatures in a theoretically consistent manner.

A variety of models fall into this category. The models proposed by Bodner and Partom (1975), Kocks (1976), Hart (1976), Miller (1976), Krieg *et al.* (1978), Anand (1982), Bammann (1984) and Lowe and Miller (1984) are among the better known ones. While the more general models incorporate at least two internal variables (typically one scalar and one tensor), the results reported here are for a version of a general model which has been simplified to include only a scalar internal variable. The constitutive equations for the shear deformations (eqn (6)) are structured then as

flow law (Levy–Mises)
$$\boldsymbol{\sigma}' = 2\mu_c \mathbf{d}' \tag{17}$$

yield criterion
$$\sigma'_{II} = \tau(d'_{II}, \theta, \kappa) \tag{18}$$

and

evolution equation
$$\frac{D}{Dt}(\kappa) = f(d'_{II}, \theta, \kappa). \tag{19}$$

An "effective" viscosity is defined from eqns (17) and (18) as

$$\mu_e = \frac{\sigma'_{II}}{3d'_{II}}. \tag{20}$$

The "effective" viscosity obviously is variable, and depends on the rate of deformation, temperature, and material state.

A number of assumptions have been made in representing the metal behavior with equations of this form. First, the metal is being treated as isotropic. In the rolling applications studied here, the plastic strains are much larger than the elastic strains and a back-extrapolated definition of the yield stress is valid. For many metals, the yield surface based on a back-extrapolated definition is approximated well by a von Mises surface provided sufficient straining has occurred. Under modest changes in loading direction large errors could result in the straining direction from an isotropic assumption. This is not considered here since the plastic strains in the rolling applications presented do not reach the large values where this is known to be important.

A second simplifying assumption is that the material does not reach such an advanced state of deformation during the forming operation that any ductility limit is exceeded. For general predictive capability, however, appropriate criteria for the transition to modes of deformation associated with failure should be checked during a simulation to ensure that the material remains within bounds for the assumed ductile mode of deformation. Another assumption that has been made in these simulations is to neglect elasticity. This is not a restriction imposed by the constitutive models, which do allow elastic strains to be added to the plastic strains to obtain the complete response. Rather, this assumption is made on the basis that the plastic strains in the forming operations studied are very much larger than the elastic strains and the loads are not reversing. As a consequence, residual stresses are not computed.

The underlying premise of internal variable models is that the response of a material to an applied load may be determined uniquely from the material's current state. The collection of internal variables completely defines the material properties and eliminates the need to remember the temperature and deformation history that brought the material to its present condition. All histories that produce the same changes in the internal variables from identical starting configurations are equivalent from the perspective of the material behavior. We have concentrated on a model that uses a single scalar variable to describe the state of the material. This implies that there is one microstructural feature that controls the rate of deformation for a particular combination of stress and temperature. Models with one internal variable are capable of following one transient in the material response associated with the evolution of the dominant microstructural feature. Other transients (associated with other microstructural features) that may occur must decay quickly in relation to the dominant transient for the single variable model to represent the material well. The usefulness of a single-variable model therefore is dependent on the existence of a dominant transient over the total span of the forming deformation being simulated. In the model used here the observed transient that the model represents is the entire stress–strain curve. Short transients that occur near the initial point of plastic yielding (such as a yield drop or Bauschinger effect) are not included.

The constitutive model proposed by Hart (1976) has been used to represent aluminum in the rolling applications presented later. Hart examined the observed laboratory behavior of aluminum alloys, stainless steels, and other metals in constructing the model. Tests on 1100 aluminum were performed at approximately $0.3\theta_m$ (Hart and Solomon, 1973).

A mechanical analogy of the model has two parallel legs; one leg having a frictional (non-hardening viscoplastic) element and the other having a series combination of an anelastic spring and a rate-dependent plastic (hardening viscoplastic) element. The frictional element represents the resistance to dislocation glide from the frictional force acting on slip planes

$$\sigma''_{II} = G_e\left(\frac{d''_{II}}{a}\right)^{1/M} \tag{21}$$

where

$$a = a_0 \exp\left(\frac{-Q'_0}{R\theta}\right). \tag{22}$$

The stress in this element generally is small in comparison to the stress in the plastic element, except at either high strain rates or low temperatures. The plastic element represents the plastic flow resistance controlled by dislocation motion past strong barriers

$$\sigma'^{\mathrm{p}}_{\mathrm{II}} = \sigma^* \exp\left[-\left(\frac{d^*}{d'^{\mathrm{p}}_{\mathrm{II}}}\right)^{\chi}\right] \tag{23}$$

where

$$d^* = f_0\left(\frac{\sigma^*}{G_e}\right)^m \exp\left(\frac{-Q_0}{R\theta}\right). \tag{24}$$

The plastic flow resistance increases with straining due to an increase in the barrier strength with the density of dislocations. The scalar internal variable quantifies this barrier strength in a continuum sense and is referred to as the hardness. The exact analytic form for this element was deduced by Hart from the scaling of stress relaxation tests for differing hardness. The form implies that the stress in the plastic element is not a monotonic function of the hardness, but rather has a maximum value at finite (non-zero) hardness. As is observed for metals deforming by slip, the strain-rate sensitivity of the flow stress of the plastic element is small at low temperatures and increases as the temperature increases. The anelastic element is responsible for the apparent anisotropy predicted by the model. The tensor strain in this element is the second internal variable and is partially recovered on unloading since it is in parallel with the (viscoplastic) frictional element. The anelastic strain is proportional to the stress acting on the leg that contains it through a modulus of the same order of magnitude as the elastic shear modulus. We have chosen to neglect this element since it describes relatively short transients (in monotonic straining) in comparison to the overall hardening observed in stress–strain curves for large strains. The evolution of the hardness is described by an equation that predicts a diminishing hardening rate for increasing hardness or decreasing (plastic element) stress

$$\frac{\mathrm{D}}{\mathrm{D}t}(\sigma^*) = c_0 \sigma^* d'^{\mathrm{p}}_{\mathrm{II}} \left(\frac{G_e}{\sigma^*}\right)^{m'} \left(\frac{\sigma'^{\mathrm{p}}_{\mathrm{II}}}{\sigma^*}\right)^n. \tag{25}$$

The hardening rate is never zero, however, if the plastic element is deforming, so that a saturation value of the hardness does not exist although the rate of hardening constantly decreases with continued straining. The form of the evolution equation for hardness proposed by Hart gives low hardening rates at high temperatures or low strain rates. At low temperatures incremental changes in the hardness resulting from increments in plastic strain are nearly independent of the strain rate. As given in eqn (25), the evolution of the hardness does not include static recovery effects. At high temperatures recovery may produce significant changes in the hardness given adequate time, as discussed earlier. In Hart's model the flow stress is a weak function of the hardness at high temperature, so modest changes in the hardness due to static recovery have little impact on the flow stress.

Because the plastic and frictional elements act in parallel, the following compatibility equations apply:

$$d'_{\mathrm{II}} = d'^{\mathrm{v}}_{\mathrm{II}} = d'^{\mathrm{p}}_{\mathrm{II}} \tag{26}$$

$$\sigma'_{\mathrm{II}} = \sigma'^{\mathrm{v}}_{\mathrm{II}} + \sigma'^{\mathrm{p}}_{\mathrm{II}}. \tag{27}$$

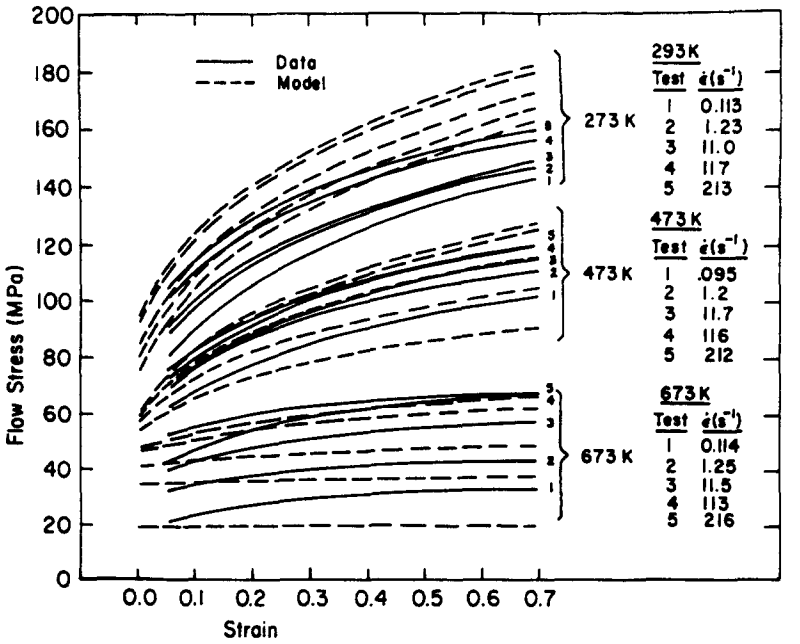

Fig. 1(a). Flow stress data for 1100 aluminum showing measured and computed responses.

These equations define the observable stress and rate of deformation in terms of the quantities acting on each leg of the mechanical analog. Equations (21)–(27) are a specific case of eqns (18) and (19).

Prior to conducting the rolling simulations, it was necessary to define values for all of the parameters in the constitutive model. Several of the values are considered well known for aluminum, namely λ, G_c, M and m, from relaxation data (Hart and Solomon, 1973). The values for Q_0 and Q'_0 were taken to be equal to the value for the activation energy reported by Sheppard and Wright (1979). The other parameter values were not known, particularly in the range of stress and temperature typical of hot or warm rolling. For this reason, the unknown material parameters were evaluated from data reported by Hockett (1976) for 1100 aluminum. The data in this article were used because the test conditions included a range of deformation rates from 10^{-1} to 10^{2} s^{-1}, homologous temperatures of 0.3–0.8, and logarithmic strains of up to 0.7. The data were obtained from cam plastometer tests that provided constant deformation rates in axial compression. The constitutive equations for the stress and the internal variable under deformations corresponding to the imposed experimental conditions were integrated numerically using various combinations of the unknown material parameters (n, m'_0, c_0, f_0, a_0, σ^*_0) until reasonable fits to the data were obtained. Figure 1(a) shows the results of fitting the simplified version of Hart's model to data reported by Hockett. Greatest weight was given to matching the curves for the intermediate temperature of 473 K. The strain rates of 11.8 and 113 s^{-1} were taken to be closest to rates typical in rolling. In this regime, the fits are quite good. However, at either higher or lower temperatures the hardening behavior predicted does not match the test data as well, even though the overall magnitudes of the stresses are reasonable. The increase in the hardness (internal variable in Hart's model) for each of the tests is shown in Fig. 1(b). At the lowest temperature, the hardening is nearly independent of deformation rate. The effect of deformation rate, however, is clearly present for the higher temperature tests. The parameters for Hart's model that were used in the simulations are given in Table 1. Fits of comparable or better quality using other values of the constants n, m', c_0, f_0, a_0, and σ^*_0 are possible. Further, by also allowing the remaining parameters (λ, M, m, Q_0, and Q'_0) to vary in fitting the models to Hockett's data considerable flexibility exists. However, establishing values for these parameters from relaxation data as was done here broadens the data base and gives more confidence in the accuracy of the parameters.

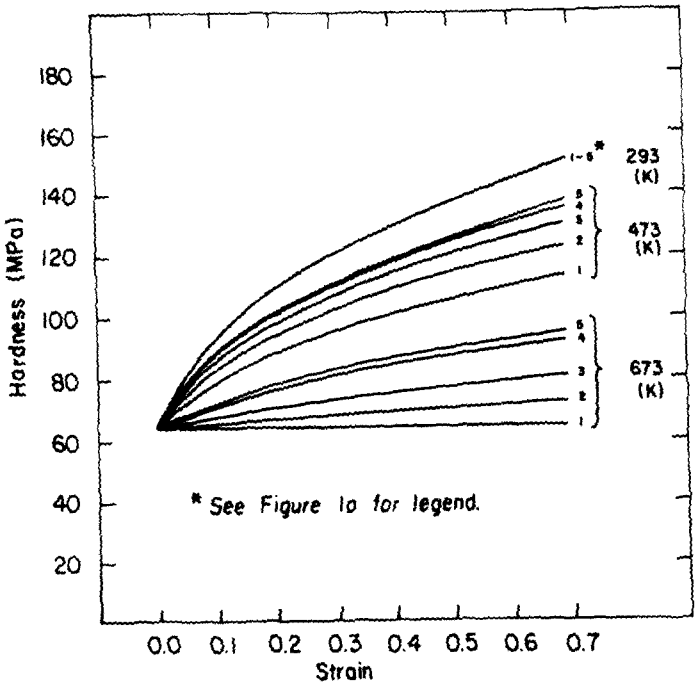

Fig. 1(b). Hardness curves for modified Hart model corresponding to 1100 aluminum flow stress curves (Fig. 1(a)).

4. NUMERICAL SOLUTION OF THE MODEL EQUATIONS

The system of equations set forth in the preceding sections are solved approximately using numerical techniques. Finite element formulations provide solutions for the steady-state velocity and temperature fields while predictor–corrector methods are employed to integrate the evolution equations for the internal variable along streamlines of the flow. As is evident from the preceding discussion, the equations for the motion, temperature and material state are closely coupled. Simultaneous solutions for the coupled sets of equations are obtained by iteratively solving each set separately using the most recent approximations of motion, temperature and material state until the solutions converge.

4.1. *Solving for the motion*

The velocity field is determined from a variational statement representing the virtual rate of work (Thompson *et al.*, 1969) that has appended the constraint condition of incompressible deformations. The corresponding Euler equations are eqns (2) and (9) and the boundary conditions of eqns (10) and (11). This variational statement can be written as

$$\delta J = \int_V \mathrm{Tr}\,(\boldsymbol{\sigma}' \cdot \delta \mathbf{d}')\,\mathrm{d}V - \int_V \rho \mathbf{g} \cdot \delta \mathbf{u}\,\mathrm{d}V - \int_{S_\sigma} \mathbf{T} \cdot \delta \mathbf{u}\,\mathrm{d}S - \delta \int_V p\,\mathrm{Tr}\,\mathbf{d}\,\mathrm{d}V. \tag{28}$$

By introducing approximating functions for the velocity and the negative of the mean stress (Lagrange multiplier, p) over a finite element as

$$\{u(\mathbf{x})\} = [N(\mathbf{x})]\{U\} \tag{29}$$

$$p(\mathbf{x}) = [N_p(\mathbf{x})]\{P\} \tag{30}$$

and eliminating the stress using the flow law (eqn (17)), the variational statement for a single element becomes

Table 1. Simplified Hart model parameters

Parameter	Units	Value
$\ln(a_0)$	$\ln(s^{-1})$	120
$\ln(c_0)$	—	−18.6
$\ln(f_0)$	$\ln(s^{-1})$	53
M	—	7.8
m	—	5.0
m'	—	3.5
n	—	6.0
G_c	GPa	18.9†
Q_0/R	K	1.89×10^4†
Q'_0/R	K	1.89×10^4†
λ	—	0.15
σ_0^*	MPa	64

† Note: The values of G_c are lower than standard handbook values while Q_0/R and Q'_0/R are higher. Other parameters compensate for these variations in the overall fits. This in part is responsible for the high values of a_0 and f_0. It is recommended that the model parameters be evaluated based on more widely accepted values of shear modulus and the activation energy for further calculations.

$$\delta J_e = \{\delta U\}_e^T[K]_e\{U\}_e - \{\delta U\}_e^T[G]^T\{P\}_e - \{\delta P\}_e^T[G]_e\{U\}_e - \{\delta U\}_e^T\{F\}_e \tag{31}$$

$$[K]_e = \int_{V_e} [N']^T[D][N']\,dV \tag{32}$$

$$[G]_e = \int_{V_e} [N_p]^T\{h\}^T[N']\,dV \tag{33}$$

$$\{F\}_e = \int_{V_e} [N]^T\{\rho g\}\,dV + \int_{S_e} [N]^T\{T\}\,dS. \tag{34}$$

Here, matrix notation has been introduced for convenience, and the spatial derivatives of the approximating functions, $[N']$, are defined to give

$$\{d\} = [N']\{U\}_e \tag{35}$$

$$\text{Tr}\,\mathbf{d} = \{h\}^T\{d\} = \{h\}^T[N']\{U\}_e. \tag{36}$$

Matrix $[D]$ is a diagonal matrix consisting of effective viscosities as defined by eqn (20). Following standard practices of the finite element method, a matrix equation is obtained for the nodal point velocities and pressures

$$\begin{bmatrix} K & G^T \\ G & 0 \end{bmatrix}\begin{pmatrix} U \\ -P \end{pmatrix} = \begin{pmatrix} F \\ 0 \end{pmatrix}. \tag{37}$$

Because the effective viscosities depend on the velocity field, this equation is nonlinear and is solved using a combination of Newton–Raphson and Picard's methods. For frictional sliding on the surface as represented by the model of eqn (12), the force matrix depends on the unknown velocity. In this case the portion of the force term containing the unknown velocities is appended to the stiffness matrix $[K]_e$ while the known quantity from the tool velocity remains in the force matrix (Dawson, 1984).

4.2. *Solving for the temperatures*

The temperature distribution is evaluated from a weighted residual formed from the energy equation and an appropriate set of weighting functions. The energy equation is first written in terms of the temperature by introducing eqns (7) and (8) and simplified to steady-state conditions. The weighted residual then can be written as

$$W = \sum_j \int_V [\text{div}\,(k\ \text{grad}\ \theta) - \rho c_p \mathbf{u} \cdot \text{grad}\ \theta + \dot{Q}] N_j\ \text{d}V. \tag{38}$$

Choosing the weighting functions to correspond to the approximating functions for the temperature within a finite element (Galerkin's technique) and requiring that the weighted residual vanish yield a matrix equation for the nodal point temperatures

$$[H]\{\theta\} + \{B\} = 0 \tag{39}$$

where

$$[H]_e = \int_{V_e} [N^*]^T [k] [N^*]\ \text{d}V + \int_{V_e} [N]^T \rho c_p \{u\}^T [N^*]\ \text{d}V \tag{40}$$

$$\{B\}_e = \int_{V_e} [N]^T \dot{Q}\ \text{d}V + \int_{S_e} [N]^T q\ \text{d}S. \tag{41}$$

Matrix $[k]$ contains the thermal conductivity and spatial derivatives of the approximating functions, $[N^*]$, are defined so that

$$\text{grad}\ \theta = [N^*]\{\theta\}_e. \tag{42}$$

The viscous dissipation is the product of the stress and rate of deformation

$$\dot{Q}^v = \text{Tr}\,(\boldsymbol{\sigma}' \cdot \mathbf{d}') \tag{43}$$

and contributes to the total heat source, $\dot{Q}$. For the convective losses over the surface, the surface integral in eqn (41) contains the unknown nodal point temperatures. This term can be appended to $[H]$, however, leaving only known quantities in $\{B\}$ (Dawson, 1984).

4.3. *Integrating the evolution of the internal variable*

Integration of the evolution equation for the internal variable can be accomplished in a Eulerian frame with any of several different approaches. For example, a weighted residual can be formed using the evolution equation and, with standard finite element methodology, nodal point values of the internal variable can be determined that define the distribution of the internal variable over the entire domain (Thompson *et al.*, 1983). It is also possible to integrate the evolution equation for individual particles along their respective streamlines through the flow field. When this is done for a sufficient number of particles within an element, the distribution of the internal variable over the element can be evaluated by collocation. Because the streamlines are characteristic lines of the evolution equation, the evolution equation may be integrated as a (nonlinear) ordinary differential equation. Identifying the streamline position and integrating the evolution equation can be done for as many points as are necessary, with each integration effectively being independent of the others. In contrast, using a Galerkin approach a (nonlinear) partial differential equation is solved for a distribution of the internal variable over the entire domain, as specified by the approximating functions. Each approach has strengths and limitations, as discussed by Agrawal and Dawson (1985). In this article the evolution of the internal variable is computed

with a streamline technique. In other applications (three-dimensional bar rolling, for example), the evolution equation for the internal variable has been solved with a Galerkin formulation (Dewhurst and Dawson, 1984).

The two basic components of the streamline integration method, when used in conjunction with a finite element solution for the velocity field, are:

(1) define the streamline position of a specific particle as it traverses the Eulerian domain;
(2) integrate the evolution equation, starting from a point with a known initial value of the internal variable.

The upstream path that passes through a given point in the Eulerian region is located by integrating the streamline velocity

$$u_s = \frac{dx_s}{dt}. \tag{44}$$

This integration can be performed numerically to give coordinate pairs that define the particle path as it moves through the domain. The evolution of the internal variable (for Hart's model) then is

$$\int d\sigma^* = \int \left[c_0 \sigma^* \left(\frac{\sigma'^{\mathrm{p}}_{\mathrm{II}}}{\sigma^*} \right)^n \left(\frac{\sigma^*}{G_c} \right)^{-m'} d'_{\mathrm{II}} \right] dt. \tag{45}$$

The time integral is transformed to a line integral along the streamline path using eqn (44) and computed numerically using the same intervals that are used to define the streamline. An Adams–Bashford–Moulton predictor–corrector method performs the numerical integration, using predictor and corrector steps at each interval along the streamline. An important computational aspect of using the streamline method is that, in evaluating the internal variable within any given element, the streamline need only be tracked to an upstream element where the internal variable has already been computed. By moving through the mesh in the direction of flow, streamline integrations are usually necessary only over the dimension of an element to define the internal variable distribution within that element. Additional details of the streamline technique are available (Dawson, 1984).

5. SLAB ROLLING APPLICATION

The rolling of aluminum slabs was simulated with the model equations and numerical algorithms presented in the preceding sections. This application was chosen for detailed study because it is commerically important and there exists some experimental data relating the rolling conditions to the mechanical properties of the resulting product (Hatch, 1984). A variety of rolling conditions were imposed on a slab of 1100 aluminum to evaluate the sensitivity of the predicted hardening behavior and temperature rises to changes in the rolling conditions.

In the rolling simulations, a slab was compressed between two rigid rolls to reduce its thickness (Fig. 2). The rolls had an outside radius of 10 cm and rotated at a constant angular velocity of 10 rad s^{-1}, making the tangential velocity of the roll surface 1 m s^{-1}. Combinations of three thickness reductions and three upstream temperatures were simulated. The thickness reductions were 10, 30, and 50%, such that slabs that were initially 4.0 cm thick were reduced to 3.6, 2.8, and 2.0 cm, respectively. The upstream temperatures were 0.5, 0.6, and $0.7\theta_m$, or 466, 560 and 673 K, respectively. In addition to these nine cases in which sticking conditions between the roll and slab were assumed, three additional cases of sliding friction were simulated, all at 30% reduction and $0.6\theta_m$ upstream temperature. The frictional coefficient, β, was varied over a wide range such that the interface conditions changed from nearly sticking to having a slab tangential velocity at the surface always less than the roll velocity. In all of the simulations, convective heat losses were included from the free surfaces and the heat loss to the rolls was modeled as convection with a very large

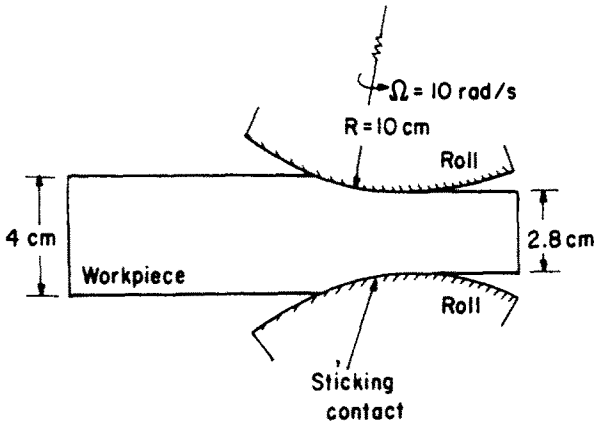

Baseline Parameters

Reduction : 30%

Workpiece Material : Aluminum

Initial Temperature : 560 K

Parameter Variations

Reduction : 10%, 50%

Initial Temperatures : 466, 673 K

Roll / Slab Contact : Sliding friction

Fig. 2. Schematic diagram of the rolling application.

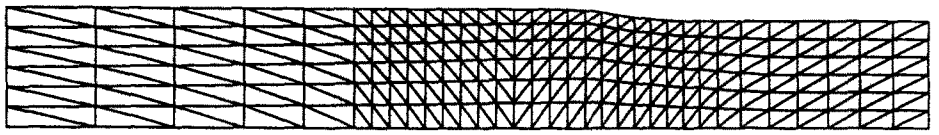

Fig. 3. Finite element mesh for rolling simulations.

film coefficient. The free surface positions were adjusted to ensure that they were streamlines of the velocity field using the spline technique discussed by Dawson (1984).

The simulations were performed using a finite element mesh having 396 isoparametric triangular elements (quadratic velocity and temperature interpolations) with 871 nodal points for the velocity and the temperature and 633 nodal points for the pressure (Fig. 3). The streamline integrations were performed using a spatial step size along a streamline of 0.1 mm. With this step size approximately 30 steps were needed to traverse the small elements inside the bite and approximately 150 steps were required to traverse the larger elements near the slab ends. Convergence criteria were set on the velocity, temperature, stress, internal variable, and rate of deformation changes between iterations of 0.1%. Convergence normally required 10–15 iterations with execution times on the University of Minnesota CRAY-1S of approximately 4–5 CPU minutes.

In the cases of sticking friction between the slab and the roll, the velocity field is largely determined by the kinematics imposed by the amount of reduction and the roll velocity. The distributions of the effective rates of deformation are shown in Fig. 4 for the intermediate temperature cases ($\theta_0 = 0.6\theta_m$).† The peak rates of deformation increase with greater reductions and are largest near the first point of contact with the roll. The largest values encountered are approximately 120 s^{-1} in the 50% reduction case. For lighter reductions of 10 and 30%, the peak rates of deformation are approximately 30 and 60 s^{-1}, respectively. These values scale approximately with the roll speed. Along the centerline of the slab the

† Contour plots of the rate of deformation and the hardness (which are computed and stored at interior points of each element) were generated after computing nodal point values with a Galerkin method. A filter was applied to these nodal point values to remove some oscillations introduced by the Galerkin procedure.

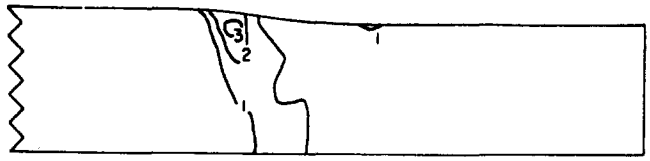

a. 10% reduction (Interval between contours = $7.5s^{-1}$; Contour 1 = $7.5s^{-1}$)

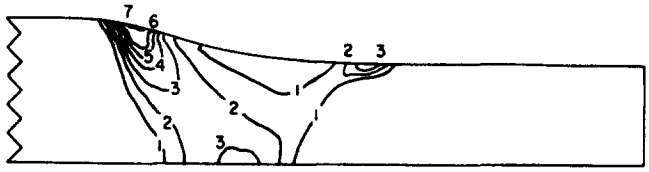

b. 30% reduction (Interval between contours = 7.5^{-1} ; Contour 1 = $7.5s^{-1}$)

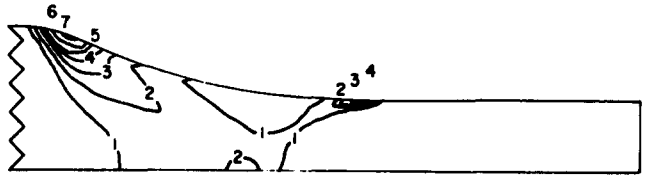

c. 50% reduction (Interval between contours = $15s^{-1}$; Contour 1 = $15s^{-1}$)

Fig. 4. Rate of deformation (d'_{ii}) contours for various reductions.

rates of deformation are considerably smaller than the surface values, only reaching 20 s^{-1} in the 30% reduction example.

The temperature contours for the three cases at $\theta_0 = 0.6\theta_m$ and sticking friction are presented in Fig. 5. Larger temperature rises are expected with greater reduction, as is evident from the figure. The higher rates of deformation near the slab surface contribute to the high heating rate and high temperatures observed there. Also the chilling effect of the rolls can be observed from the isotherms that are approximately parallel to the roll surface, indicating an overall heat flux in the direction of the roll.

The hardness (internal variable) evolves most quickly in the regions of high rate of deformation. This is shown in Fig. 6 where the hardness is plotted for three material particles as a function of the position along the slab. Near the surface the hardness climbs very rapidly as a particle passes through the zone of greatest rates of deformation. The hardness remains relatively constant while the particle is close to the roll and the rates of deformation are constrained by the sticking friction condition. The hardness further increases when the particle passes through the region at the end of the slab/roll contact where material also is deforming rapidly. Near the centerline the rates of deformation are lower and change more gradually. The hardness increases smoothly along this path, but reaches a smaller value than is computed for particles near the surface. This implies a hardness gradient from the core to the surface of the slab.

The distribution of hardness of the deforming slab is shown for the various reductions (at $\theta_0 = 0.6\theta_m$) in Fig. 7. It is clear that larger reductions induce greater hardening, as would be expected. The effect of changing the upstream temperature at fixed reduction is shown in Fig. 8. Lower temperatures induce greater hardening since the evolution of the hardness depends on the stress which, in turn, changes with temperature. The larger amounts of hardening near the surface are evident in both Figs 7 and 8.

The results of the above simulations and other sticking friction cases have been summarized in Figs 9 and 10. In Fig. 9(a), the surface hardness (normalized by the

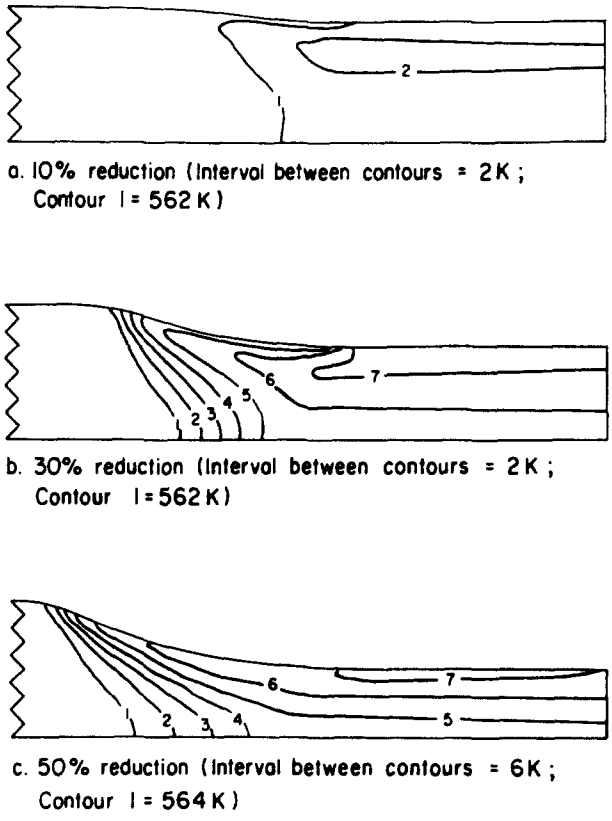

Fig. 5. Temperature contours for various reductions.

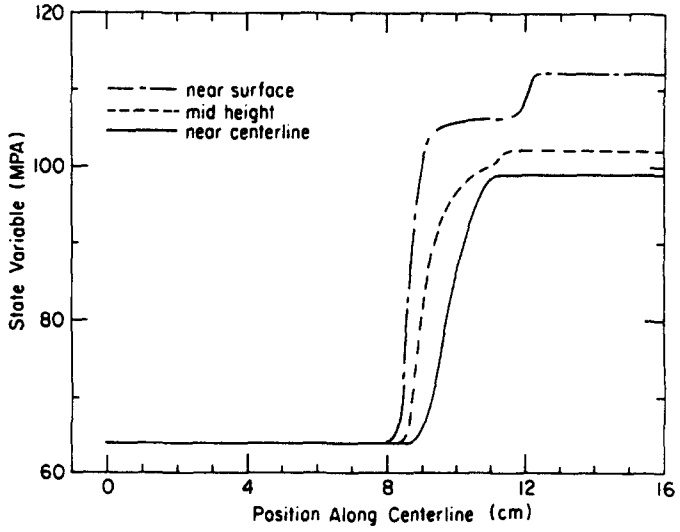

Fig. 6. Hardness (σ^*) vs distance along the centerplane (x) for various streamlines.

initial hardness) has been plotted as a function of the reduction for the three upstream temperatures. The hardness increases with higher temperature or larger reduction, as stated earlier. The relative changes in hardness are significant. In the most severe case of a 50% reduction and an upstream temperature of $0.5\theta_m$, the hardness increases by a factor of 2.70. At temperatures above $0.5\theta_m$, it is likely that recovery in the hot slab reduces the levels of hardness induced by rolling. This does not imply, however, that hardening during the rolling need not be included in the forming model. Even though the effects of hardening may later be removed partially by recovery, the stresses during rolling are higher as a result of hardening.

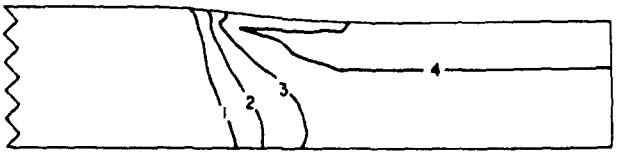

a. 10% reduction (Interval between contours = 6 MPa ; Contour 1 = 66 MPa)

b. 30% reduction (Interval between contours = 12 MPa ; Contour 1 = 66 MPa)

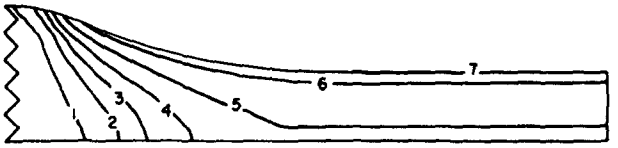

c. 50% reduction (Interval between contours = 12 MPa ; Contour 1 = 66 MPa)

Fig. 7. Hardness (σ^*) contours for various reductions.

a. θ_0 = 466 K (Interval between contours = 12 MPa; Contour 1 = 66 MPa)

b. θ_0 = 560 K (Interval between contours = 12 MPa; Contour 1 = 66 MPa)

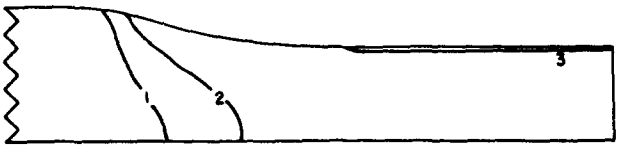

c. θ_0 = 673 K (Interval between contours = 12 MPa ; Contour 1 = 66 MPa)

Fig. 8. Hardness (σ^*) contours for various initial temperatures.

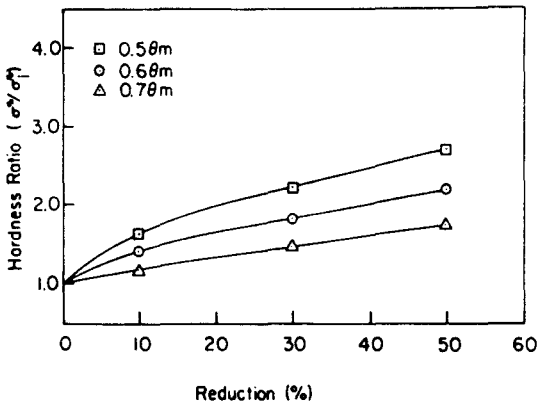

Fig. 9(a). Hardness (σ^*) vs reduction.

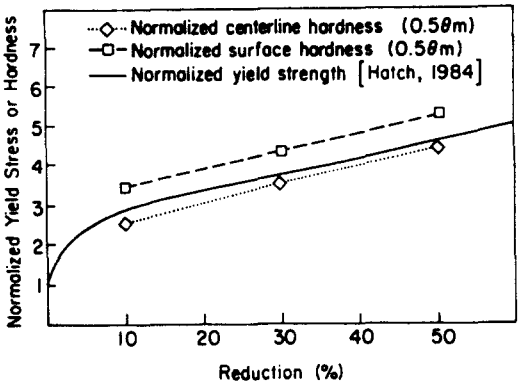

Fig. 9(b). Yield stress–hardness comparison for slabs rolled to various reductions.

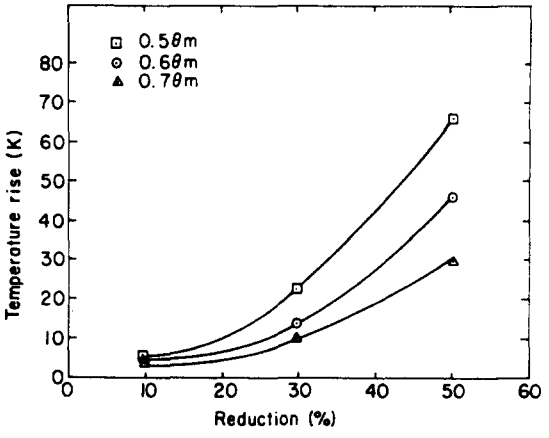

Fig. 10. Temperature rise ($\Delta\theta$) vs reduction.

The computed changes in hardness for the lowest temperature simulations are compared to measured yield strength data (Hatch, 1984) for cold rolled 1100 aluminum plate in Fig. 9(b). Here, both the yield strength and hardness values have been normalized by the 0% reduction yield strength value (~32 MPa) reported by Hatch (1984). The surface hardness values are greater than the yield strengths, but both increase with reduction at very similar rates between the range of reductions (10–50%) analyzed. The centerline hardness values are less than the corresponding computed surface values and compare closely to the measured yield strengths. It should be noted that simulations performed at lower temperatures than reported here do not predict appreciably larger hardness increases. The increase in hardness diminishes as the initial temperature decreases. For example, an additional 30% reduction simulation performed at $\theta_0 = 373$ K ($0.4\theta_m$) resulted in a surface hardness which was only about 10% larger than the $\theta_0 = 466$ K ($0.5\theta_m$) surface hardness.

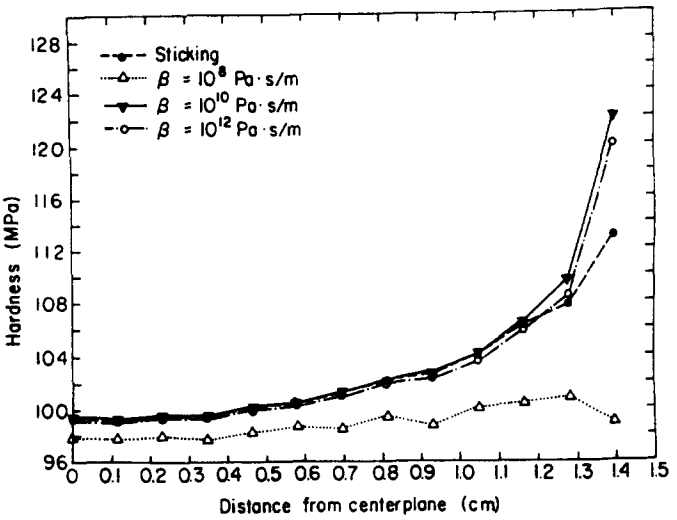

Fig. 11. Hardness (σ^*) vs distance from the centerplane (y) for various friction coefficients β.

This is because the ratio $\sigma^*/\sigma_{11}^{\prime p}$ approaches unity as temperatures diminish. It is clear from Fig. 9(b) that the relative changes in the hardness are a good indication of the changes in yield strength that would be expected due to the rolling process.

The computed temperature rises are shown in Fig. 10 as a function of the reduction for various upstream temperatures. Larger reductions at lower temperatures cause greater temperature rises, as would be expected. The significance of the calculations is that at lower temperatures an isothermal assumption would be poor for large reductions because the induced temperature changes could substantially change the flow properties. In applications having light reductions, such as the 10% case, the temperature changes are modest and have little impact on the properties. The overall temperature rises are comparable to those reported for a purely viscoplastic (hyperbolic) constitutive model (Dawson, 1984). A linear interpolation between $0.6\theta_m$ and $0.7\theta_m$ at 50% reduction in Fig. 10 to estimate the temperature rise for $0.64\theta_m$ (600 K), as was used in Dawson (1984), gives a temperature rise of approximately 38 K, compared to 36 K computed for the viscoplastic model. This small difference cannot be attributed solely to differences in the form of the constitutive models, however, since the same data were not used to evaluate the parameter values and the finite element meshes were not identical (much finer resolution was used here).

Differences in the assumed frictional conditions between the rolls and the slab were also examined. Besides sticking friction discussed in the previous cases, three sliding friction conditions were considered. In one a very large value of the friction coefficient, β, was chosen (10^{12} Pa s m^{-1}) so that a condition very near sticking friction was achieved. The other two had lower friction coefficients (10^{10} and 10^{8} Pa s m^{-1}) such that, in the case of the lowest coefficient, the slab never reaches the roll surface velocity. To illustrate the differences between the various cases the hardness and temperature throughout the product slab have been plotted (Figs 11 and 12). The temperatures near the surface are somewhat higher for sliding friction with $\beta = 10^{10}$ Pa s m^{-1} than for the case of sticking friction. However, when $\beta = 10^{8}$ Pa s m^{-1} (the lowest value considered) the temperatures are below any of the other cases and are more uniform through the thickness. The initial temperature was 560 K in every case, so the differences in temperature between the various cases are generally smaller than the average temperature rise (approximately 15 K). The hardness changes show similar trends to the temperature. Sliding friction causes the hardness to be somewhat larger than for sticking friction, except in the lowest friction coefficient case in which the hardnesses are smaller and more uniform through the slab.

6. SUMMARY

The steady-state rolling of aluminum slabs has been studied with a forming model that includes constitutive equations for the rate-dependent plastic flow of aluminum. Simulations

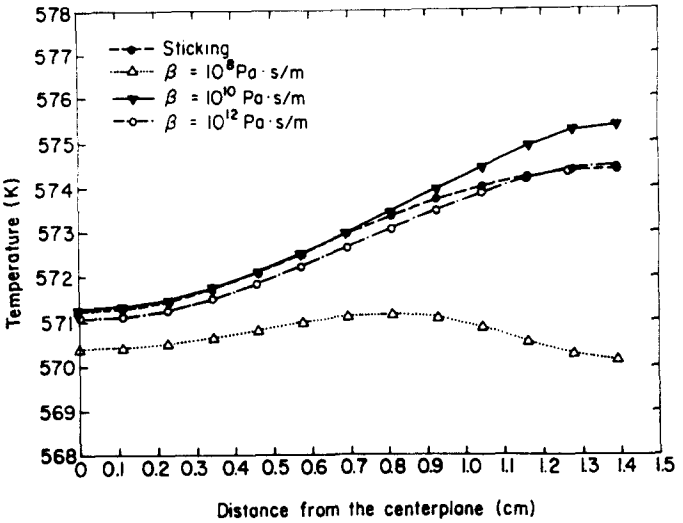

Fig. 12. Temperature rise ($\Delta\theta$) vs distance from the centerplane (y) for various friction coefficients β.

were performed over a broad range of rolling conditions, spanning reductions from 10 to 50% and initial temperatures from 0.5 to 0.7 of the melt temperature. Hardening behavior was represented with the internal variable model developed by Hart. Parameters for this constitutive model were evaluated by fitting the model to constant rate of deformation data reported by Hockett. The forming model equations were solved numerically by a combination of finite element and predictor–corrector integration methods.

The simulations demonstrate that the internal variable representation for the plastic flow can be used to compute how the mechanical properties, as quantified by the internal variable, vary with the imposed rolling conditions. In these simulations the increases in hardness and the temperature rises were both larger for greater reduction or lower initial temperature. Changing the slab/roll interface friction condition altered the slab response, increasing the hardness for small degrees of sliding and reducing it for larger amounts of sliding. Comparisons of the relative changes in hardness with measured yield strengths for rolled products show the model is capturing the essence of the hardening behavior during rolling.

Acknowledgements—The author is indebted to U. F. Kocks, J. Lipkin and E. G. Thompson for their helpful comments in preparing this paper. The author also wishes to thank K. Mathur and G. M. Eggert for their assistance in preparing the figures and Glenda Seliga for assistance in preparing the manuscript. The author is indebted to the National Science Foundation for its support of this research under grants MEA-8105605 and DMC-8352275. The author would also like to thank General Motors Corporation and Deere & Company for their generous support of this research.

REFERENCES

Agrawal, A. and Dawson, P. R. (1985). A comparison of Galerkin and streamline techniques for integrating strains from an Eulerian flow field. *Int. J. Numer. Meth. Engng* **21**, 853.

Anand, L. (1982). Constitutive equations for the rate-dependent deformation of metals at elevated temperatures. *ASME J. Engng Mater. Technol.* **104**, 12.

Argyris, J. H., Doltsinis, J. St., Knudson, W. C., Szimmat, J., Willam, K. J. and Wüstenberg, H. (1980). Eulerian and Lagrangian techniques for elastic and inelastic large deformation processes. *Computational Methods in Nonlinear Mechanics* (Edited by J. T. Oden), Chap. 2, p. 13. North-Holland, Amsterdam.

Bammann, D. J. (1984). An internal variable model of viscoplasticity. *Int. J. Engng Sci.* **22**, 1041.

Bodner, S. R. and Partom, Y. (1975). Constitutive equations for elastic–viscoplastic strain-hardening materials. *Trans. Am. Soc. Mech. Engrs*, Section E, *J. Appl. Mech.* **42**, 385.

Chandra, A. and Mukherjee, S. (1984). A finite element analysis of metal forming problems with an elastic–viscoplastic material model. *Int. J. Numer. Meth. Engng* **20**, 1613.

Cook, P. M. (1957). True stress–strain curves for steel in compressions at high temperatures and strain rates, for application for the calculation of load and torque in hot rolling. *Proceedings of the Conference on Properties of Materials at High Rate of Strain*. IME, 86.

Dawson, P. R. (1980). Viscoplastic modeling of upset welding using the finite element method. *Process Modeling Tools, Proc. of ASM 1980 Process Modeling Sessions Materials and Processes Congress*, p. 151.

Dawson, P. R. (1984). A model for the hot or warm forming of metals with special use of deformation mechanism maps. *Int. J. Mech. Sci.* **26**(4), 227.

Dawson, P. R. and Thompson, E. G. (1977). Steady state thermomechanical finite element analysis of elasto-viscoplastic metal forming processes. *Numer. Modelling Mfg Processes.* ASME, PVP-PB-025, 167.

Dewhurst, T. B. and Dawson, P. R. (1984). Analysis of large plastic deformations at elevated temperatures using state variable models. *Constitutive Equations: Macro and Computational Aspects, Proceedings of the ASME 1984 WAM Symposium on Constitutive Equations: Micro, Macro, and Computational Aspects*, p. 149.

Eggert, G. M. and Dawson, P. R. (1987). Assessment of a thermoviscoplastic model of upset welding by comparison to experiment. *Int. J. Mech. Sci.* **28**(9), 563.

Estivalet, M. C., Jovanique, D., Chenot, J. L., Siener, P. and Faessel, A. (1982). Hot rolling: spread of blooms. *J. Méc. Theor. Appl.* **1**(1), 147.

Flower, E. C. and Hallquist, J. O. (1986). Computer-aided simulation of metal forming. Univ. of California, Lawrence Livermore National Laboratory Report # UCRL-93634.

Hart, E. W. (1976). Constitutive relations for the nonelastic deformation of metals. *Trans. Am. Soc. Mech. Engrs, J. Engng Mater. Technol.* **98**, 193.

Hart, E. W. and Solomon, H. D. (1973). Load relaxation studies of polycrystalline high purity aluminum. *Acta Metall.* **21**(3), 295.

Hatch, J. E., Editor (1984). *Aluminum: Properties and Physical Metallurgy.* American Society for Metals, Metals Park, Ohio.

Hecker, S. S. and Stout, M. G. (1984). Strain hardening of heavily cold worked metals. *Deformation Processing and Structure, Proceedings of 1982 ASM Materials Science Seminar* (Edited by G. Krauss). ASM, 1.

Hibbit, H. D., Marcal, P. V. and Rice, J. R. (1970). A finite element formulation for problems of large strain and large displacement. *Int. J. Solids Structures* **6**, 1069.

Hockett, J. E. (1976). On relating the flow stress of aluminum to strain, strain-rate, and temperature. *Trans. Metall. Soc. AIME* **239**, 969.

Key, S. W., Krieg, R. D. and Bathe, K.-J. (1979). On the application of the finite element method to metal forming processes. *Comput. Meth. Appl. Mech. Engng* 17.

Kiefer, B. V. (1984). Three-dimensional finite element prediction of material flow and strain distribution in rolled rectangular billetts. 1st Int. Conf. on Tech. of Plasticity, 3–7 Sept., Tokyo, Japan.

Kiefer, B. V. and Hilton, P. D. (1985). Combined viscous and plastic deformations in two-dimensional large strain finite element analyses. *Trans. Am. Soc. Mech. Engrs, Engng Mater. Technol.* **107**, 13.

Kobayashi, S. (1985). Metal forming and the finite element method—past and future, preprint.

Kocks, U. F. (1976). Laws for work-hardening and low temperature creep. *Trans. Am. Soc. Mech. Engrs, J. Engng Mater. Technol.* **98**, 76.

Krieg, R. D., Swearengen, J. C. and Rhode, R. W. (1978). A physically-based internal variable model for rate-dependent plasticity. *Inelastic Behavior of Pressure Vessels and Piping Components*, ASME PVP-PB-028, p. 15.

Lee, E. H., Mallett, R. L. and McMeeking, R. M. (1977a). Stress and deformation analysis of metal forming processes. *Numerical Modelling in Manufacturing Processes* (Edited by R. F. Jones, Jr., H. Armen and J. T. Fong), ASME PVP-PB-025, p. 19.

Lee, E. H., Mallett, R. L. and Yang, W. H. (1977b). Stress and deformation analysis of the metal extrusion process. *Comput. Meth. Appl. Mech. Engng* **10**, 339.

Li, J. L. and Kobayashi, S. (1981). Rigid plastic finite element analysis of plane strain rolling. ASME Paper No. 81-WA/PROD 13.

Li, J. L. and Kobayashi, S. (1984). Analyses of spread in rolling by the rigid-plastic, finite element method. *Numerical Analysis of Forming Processes.*

Lowe, T. C. and Miller, A. K. (1984). Improved constitutive equations for modeling strain softening, part I: conceptual development and part II: predictions for aluminum. ASME 84-WA/MATS 15 and 16.

McMeeking, R. M. and Rice, J. R. (1975). Finite-element formulations for problems of large elastic plastic deformation. *Int. J. Solids Structures* **11**, 601.

McQueen, H. J., Petkovic, R., Weiss, H. and Hinton, L. G. (1975). Flow stress and microstructural changes in austenitic stainless steel during hot deformation. AIME Seminar on Hot Deformation of Austenite, Cincinnatti, Ohio.

Miller, A. K. (1976). An inelastic constitutive model for monotonic, cyclic and creep deformation: part I–II. *Trans. Am. Soc. Mech. Engrs, J. Engng Mater. Technol.* **98**, 97.

Mori, K., Osakada, K. and Oda, T. (1982). Simulation of plane-strain rolling by the rigid-plastic finite element method. *Int. J. Mech. Sci.* **24**(9), 519.

Needleman, A. (1972). Void growth in an elastic–plastic medium. *J. Appl. Mech.* **39**, 964.

Needleman, A. (1982). Finite elements for finite strain plasticity problems. *Plasticity of Metals at Finite Strain: Theory, Computational, and Experiment* (Edited by E. H. Lee and R. L. Mallett), pp. 387–436. Div. Appl. Mech. Stanford University and Dept. Mech. Engng Rensselaer Poly. Inst.

Needleman, A. and Tvergaard, V. (1983). Finite element analysis of localization in plasticity. *Finite Elements—Special Problems in Solid Mechanics* (Edited by J. T. Oden and G. F. Carey), Chap. 5, pp. 94–157. Prentice-Hall, Englewood Cliffs, New Jersey.

Peirce, D., Asaro, R. J. and Needleman, A. (1983). Material rate dependence and localized deformation in crystalline solids. *Acta Metall.* **31**, 1951.

Rebelo, N. and Kobayashi, S. (1980a). A coupled analysis of viscoplastic deformation and heat transfer, I: theoretical considerations. *Int. J. Mech. Sci.* **22**, 699.

Rebelo, N. and Kobabyashi, S. (1980b). A coupled analysis of viscoplastic deformation and heat transfer, II: applications. *Int. J. Mech. Sci.* **22**, 707.

Sheppard, T. and Wright, D. S. (1979). Determination of flow stress: part 1. Constitutive equation for aluminum alloys at elevated temperature. *Metals Technol.* 215.

Swearengen, J. C., Lowe, T. C. and Lipkin, J. (1985). Constitutive equations for rate-dependent plasticity. *A. Rev. Mater. Sci.* **15**, 249.

Thompson, E. G., Mack, L. R. and Lin, F.-S. (1969). Finite element method for incompressible slow viscous flow with a free surface. *Dev. Mech.* **5**, 93.

Thompson, E. G., Pittman, J. F. T. and Zienkiewicz, O. C. (1983). Some integration techniques for the analysis of viscoelastic flows. *Int. J. Numer. Meth. Fluids* **3**, 165.

Zienkiewicz, O. C., Onate, E. and Heinrich, J. C. (1981). A general formulation for coupled thermal flow of metals using finite elements. *Int. J. Numer. Mech. Engng* **17**, 1487.